Chapter 3
Nonlinear Prediction Surfaces for Estimating the Structural Response of Naval Vessels

Alysson Mondoro, Mohamed Soliman, and Dan M. Frangopol

Abstract Structural health monitoring (SHM) of naval vessels is essential for assessing the performance of the structure and the fatigue damage accrued over the service life. The direct integration of available SHM data may be useful in reducing the epistemic uncertainties arising from inaccuracies in the modeling and the variations in the as-built structural configuration from the initial design. Based on SHM data, fatigue damage indices can be predicted by implementing cell based approaches, such as the lifetime weighted sea method, that discretizes the operational conditions of the vessel into cells with specific wave height, heading angle, and speed. The integration of SHM data into the fatigue assessment using lifetime weighted sea method requires a complete set of data that covers the whole operational spectrum. However, technical malfunctions or discrete monitoring practices generate incomplete data sets. This paper proposes nonlinear prediction surfaces to estimate the ship structural response in unobserved cells based on available cell data. Expected theoretical variations of the structural response to changes in wave height, heading angle, and vessel speed are integrated in the development of the prediction surface. The proposed methodology is illustrated on the SHM data from a high speed aluminum catamaran.

Keywords Fatigue • Aluminum vessels • Structural health monitoring • Missing data • Nonlinear prediction

3.1 Introduction

SHM data can aid in the life-cycle management of structures by helping to identify the discrepancies between predicted and observed performance. The recorded SHM data provides an indication of the as-built condition of the ship and any variations in observed response from anticipated design conditions [1]. In both civil and marine structures, SHM data can be used to update design estimates for expected loads, structural responses, and fatigue life evaluation [2–5]. Fatigue cracking is a major concern in the life-cycle management of naval vessels. The constant fluctuations in loading, induced by the natural variability in sea surface, contributes to damage accumulation in fatigue sensitive details. If the observed conditions deviate substantially from their predicted values, fatigue damage may be either (a) significantly less than expected and lead to unnecessary and costly inspections, or (b) significantly higher than expected and may induce catastrophic failure with high consequences.

The lifetime weighted sea method, used to assess the fatigue life, is developed around the assumption that the operational condition can be discretized into cells where the response in each cell is stationary [6]. A cell is defined by a set of operational conditions which include wave height, ship speed, and heading angle. The total response is the summation of the response in each cell weighted by the probability of occurrence of the cell [7]. The prediction of fatigue life thus requires information to be available for all cells.

Missing data is a problem inherent in the use of SHM for fatigue analysis. First, discrete monitoring practices, while useful in limiting financial costs [8], can lead to some operational states (i.e., cells) not being recorded. Second, technical malfunctions can result in missing or unreliable data [9]. Lastly, even if data is recorded for all cells in the current operational theatre, the future operational conditions may not be similar to past ones; thus, there may be cells in the future profile that can be considered as missing data. Zhu [10] and Mondoro et al. [11] have begun to address the problem of missing data with respect to the structural response characterization of naval vessels. Linear surfaces were used to relate the operational

A. Mondoro • D.M. Frangopol (✉)
Department of Civil and Environmental Engineering, ATLSS Engineering Research Center,
Lehigh University, 117 ATLSS Dr., Bethlehem, PA 18015-4729, USA
e-mail: Dan.frangopol@lehigh.edu

M. Soliman
School of Civil and Environmental Engineering, College of Engineering, Architecture and Technology,
Oklahoma State University, 207 Engineering South, Stillwater, OK 74078-5033, USA

R. Barthorpe et al. (eds.), *Model Validation and Uncertainty Quantification, Volume 3*,
Conference Proceedings of the Society for Experimental Mechanics Series, DOI 10.1007/978-3-319-54858-6_3

conditions (i.e. wave height, ship speed, and heading angle) to a structural response characteristic. The linear surface is useful for the ease of implementation. Additionally, it requires only a minimal amount of prediction model parameters to be estimated which limits the variations that arise based on availability of data. However, the linear surfaces lack a theoretical foundation.

This paper proposes a nonlinear surface for use in predicting unobserved data. The prediction is based on the theoretical relationship between operating conditions and the structural response given as a function of the vertical bending moment. Available data is discretized into cells, the low and high frequency content are separated and fit with response parameters as detailed in [11], and the goodness-of-fit of the theoretically-based nonlinear prediction surface is evaluated and compared with that of the linear surface. Furthermore, the performance of the theoretically-based nonlinear prediction surface is evaluated for several cases with different percentage of missing data. The methodology is applied to the SHM data obtained during the seakeeping trials of the HSV-2 Swift.

3.2 Available Data and Analysis

The full stress time-history of a structural detail is a nonstationary random process due to the exposure to various loading conditions associated with sea states, routes, and speeds. However, the full stress time-history response can be discretized into cells based on wave height H_s, ship speed V, and heading angle β [6]. This discretization leads to stationary processes for the stress time-history in each cell, for which the response spectrum can be estimated. Mondoro et al. [11] proposed that the SHM response spectrum can be fit with functional forms developed from wave spectra. The low and high frequency components were fit separately in order to account for the following actions: wave loads for low frequency, and slamming for high frequency. The Pierson-Moskowitz wave spectrum and the Joint North Sea Wave Observation Project (JONSWAP) were included as two representative wave spectra. The generalized variations of the Pierson-Moskowitz spectrum and the JONSWAP spectrum take the form [11]

$$S^{+}_{PM_{GEN}}(\omega) = \frac{A_{LF}}{\omega^5} e^{-B_{LF}\omega^{-4}} + \frac{A_{HF}}{\omega^5} e^{-B_{HF}\omega^{-4}} \tag{3.1}$$

$$S^{+}_{JONSWAP_{GEN}}(\omega) = \frac{C_{LF}}{\omega^5} \exp\left(-\frac{5}{4} {D_{LF}}^4 \omega^{-4}\right) {E_{LF}}^{\exp\left(-\frac{(\omega-D_{LF})^2}{2{D_{LF}}^2\sigma^2}\right)} + \frac{C_{HF}}{\omega^5} \exp\left(-\frac{5}{4} {D_{HF}}^4 \omega^{-4}\right) {E_{HF}}^{\exp\left(-\frac{(\omega-D_{HF})^2}{2{D_{HF}}^2\sigma^2}\right)} \tag{3.2}$$

where A_{LF} and B_{LF} are fitting parameters for the low frequency content and A_{HF} and B_{HF} are fitting parameters for the high frequency content of the complete generalized Pierson-Moskowitz function, $S^{+}_{PM_{GEN}}$; and C_{LF}, D_{LF}, and E_{LF} are the fitting parameters for the low frequency content and C_{HF}, D_{HF}, and E_{HF} are fitting parameters for the high frequency content of the complete generalized JONSWAP function,$S^{+}_{JONSWAP_{GEN}}$.

3.3 Development of Theoretical Prediction Surfaces

Discrete monitoring practices and technical malfunctions contribute to the missing data problem inherent in SHM. This presents a significant challenge in the fatigue analysis of naval vessels, which is dependent on complete data sets. Linear prediction surfaces have been employed in [10, 11] to relate structural response to wave height, ship speed, and heading angle. The linear prediction surface, Ψ^{lin}, is defined as

$$\Psi^{lin} = p_1 H_s + p_2 V + p_3 \cos(\beta) \tag{3.3}$$

where H_s is the wave height, V is the ship speed, and β is the heading angle. The linear surface is included in this paper for comparison purposes. The following subsections present the development of the theoretically-based nonlinear prediction surfaces. The discussion is framed around the HSV-2 Swift but is readily applicable to other naval vessels.

3.3.1 Operational Conditions and Theoretical Response

The theoretical relationship between the operational condition (i.e., wave height, ship speed, and heading angle) and ship response (i.e., vertical bending moment) is developed by investigating the response spectrum. For naval vessels, response spectrum can be decomposed into the wave spectrum and a transfer function which quantifies the structural response to a unit sinusoid at each frequency. The response spectrum for vertical bending moment S_{VBM} is defined as

$$S_{VBM}(\omega) = [\Phi_m]^2 S_\xi(\omega) \tag{3.4}$$

where Φ_m is the transfer function for vertical bending moment and S_ξ is the wave spectrum. There are many available forms for the wave spectrum. This paper uses the Pierson-Moskowitz wave spectrum [12]

$$S_{PM}(\omega) = \frac{\alpha g^2}{\omega^5} \exp\left(-\frac{5}{4}\left(\frac{\omega}{\Omega}\right)^{-4}\right) \tag{3.5}$$

where α is 8.10×10^{-3}, g is the gravitational constant (9.81 m/s^2), and Ω is the wave frequency. It is assumed that the general relationship between the wave frequency and wave height is $\Omega = 0.14\, g/U_{19.5}$ [12] where $U_{19.5} = (H_s/0.021)^{0.5}$ [13].

The transfer function for the vertical bending moment is derived using linear strip theory for a box shaped vessel [14]

$$\Phi_m = \kappa \frac{1 - kT}{(k_e L)^2}\left[1 - \cos\left(\frac{k_e L}{2}\right) - \frac{k_e L}{4}\sin\left(\frac{k_e L}{2}\right)\right] F_v F_c \sqrt[3]{|k\cos\beta|} \tag{3.6}$$

$$F_v = 1 + 3{F_n}^2 \tag{3.7}$$

$$F_c = (1 - \vartheta)^2 + 0.6\left(1 - F_n\sqrt{kL}\cos\beta\right)(2 - \vartheta) \tag{3.8}$$

$$F_n = \frac{V}{\sqrt{g_o L}} \tag{3.9}$$

$$k_e = |k\cos\beta| \tag{3.10}$$

$$\kappa = \exp(-k_e T) \tag{3.11}$$

where k is the wave number, which for deep water waves, $k \approx \omega^2/g$, T is draught of the ship, L is length of the ship, g_o is a general characteristic of the external field, and ϑ is a function of the block coefficient C_b [15].

The response spectrum for vertical bending moment is thus related to the significant wave height H_s through the wave spectrum, and, to β and V through the theoretical transfer function for vertical bending moment. The most probable extreme value for the response can be estimated as [6]

$$Q_p = \sqrt{2m_0 \ln\left(\frac{1800T}{\pi}\sqrt{\frac{m_2}{m_0}}\right)} \tag{3.12}$$

where m_0 and m_2 are the 0th and 2nd spectral moments, where the n^{th} spectral moment, m_n, of a spectrum, S_R, is defined as

$$m_n = \int_0^\infty \omega^n S_R(\omega)\, d\omega \tag{3.13}$$

The most probable vertical bending moment, M_p, can be related to H_s, V, and β. Figure 3.1 illustrates the procedure for developing the relationship between ship speed and the most probable vertical bending moment for the HSV-2 Swift using information from Brady et al. [16]. The ship speed is varied and ${\Phi_m}^2$ is calculated based on Eq. (3.6) (Fig. 3.1a). It is important to note that H_s, V, and β are assumed to be uncoupled in regards to M_p. Therefore, only a single parameter of $\{H_s, V, \text{and } \beta\}$ is varied at a time. Figure 3.1b shows the wave spectrum. Since S_{PM} is not a function of V, all lines depicting

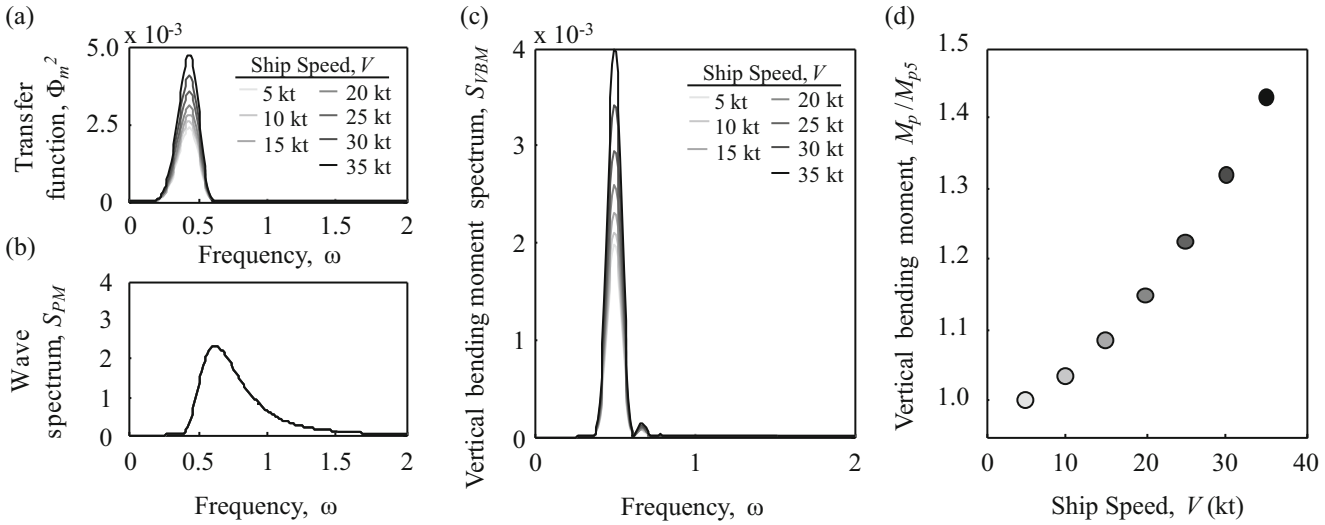

Fig. 3.1 The variations in the (**a**) transfer function $\Phi_m{}^2$, (**b**) wave spectrum S_{PM}, (**c**) response spectrum S_{VBM}, and (**d**) moment M_p/M_{p5} to changes in the speed of the ship

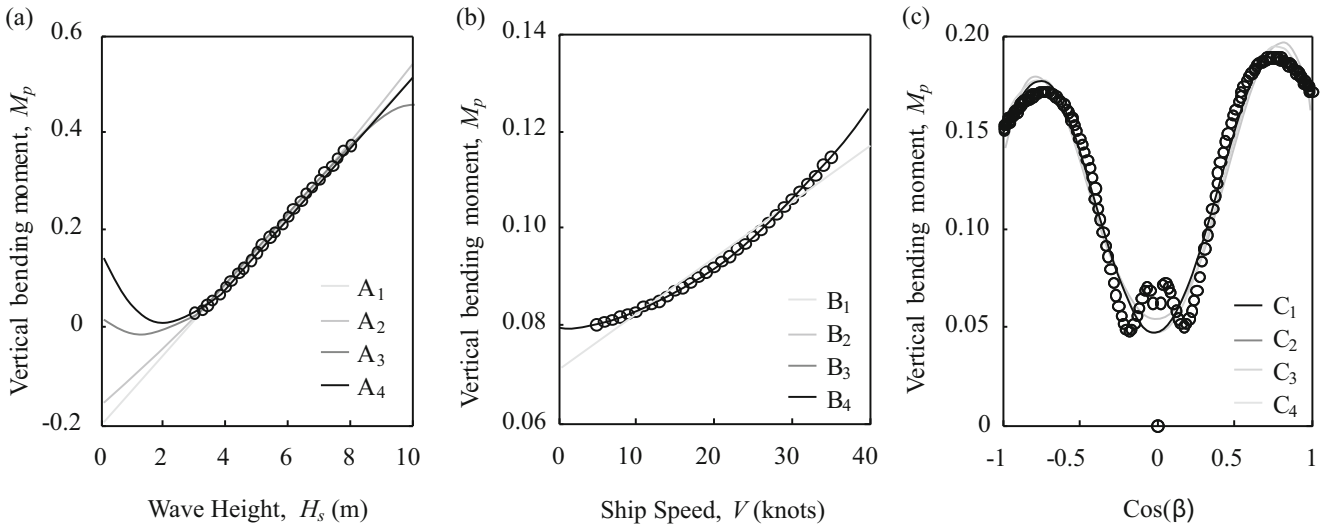

Fig. 3.2 Theoretical variations of bending moment with (**a**) wave height, (**b**) ship speed, and (**c**) heading angle (the theoretical values are shown as *black circles* and proposed functional forms are fit to each and shown as *solid lines*)

the variation of S_{PM} with V lie on top of each other. The response spectrum S_{VBM} is generated for each value of V using Eq. (3.4) and is shown in Fig. 3.1c. S_{VBM} is then used in Eqs. (3.12) and (3.13) to find the most probable vertical bending moment. The variation of M_p and V is depicted in Fig. 3.1d; the vertical bending moment at each ship speed is compared to the vertical bending moment at ship speed of 5 knots, M_{p5}. The same procedure is applied for H_s and β but figures are omitted for brevity.

3.3.2 Development of Functional Forms

A closed-form function to describe theoretical relationship between the operational condition (i.e., H_s, V, and β) and the response (i.e., M_p) is not readily available. As noted in Sect. 3.1, H_s, V, and β are assumed to be uncoupled in regards to M_p; therefore, M_p (H_s, V, β) can be decoupled into M_p (H_s), M_p (V), and M_p (β). The theoretical variations of bending moment with wave height, ship speed, and cosine of the heading angle are shown in Fig. 3.2a–c respectively. Four functional forms were developed for M_p (H_s), M_p (V), and M_p (β) and are listed in Table 3.1. Polynomial functions were used to describe M_p

Table 3.1 Proposed forms for $M_p\ (H_s)$, $M_p\ (V)$, and $M_p\ (\beta)$ and the Root Mean Square Error

Name	Form for $M_p\ (H_s)$	Root mean square error
A_1	$p_1 H_s + p_0$	0.0047
A_2	$p_2 {H_s}^2 + p_1 H_s + p_0$	0.0034
A_3	$p_3 {H_s}^3 + p_2 {H_s}^2 + p_1 H_s + p_0$	0.0007
A_4	$p_4 {H_s}^4 + p_3 {H_s}^3 + p_2 {H_s}^2 + p_1 H_s + p_0$	0.0001
Name	Form for $M_p\ (V)$	Root mean square error
B_1	$p_1 V + p_0$	0.0018
B_2	$p_2 V^2 + p_1 V + p_0$	3.78E−05
B_3	$p_3 V^3 + p_2 V^2 + p_1 V + p_0$	3.77E−09
B_4	$p_4 V^4 + p_3 V^3 + p_2 V^2 + p_1 V + p_0$	8.92E−11
Name	Form for $M_p\ (\beta)$	Root mean square error
C_1	$p_1 \sin(p_2 \cos(\beta) + p_3) + p_4 \sin(p_5 \cos(\beta) + p_6)$	0.0083
C_2	$p_1 \cos(\cos(\beta)) - p_2 \cos(p_3 \cos(\beta)) + p_4 \cos(\beta)$	0.0086
C_3	$p_4 \cos(\beta)^4 + p_3 \cos(\beta)^3 + p_2 \cos(\beta)^2 + p_1 \cos(\beta) + p_0$	0.0107
C_4	$p_6 \cos(\beta)^6 + p_5 \cos(\beta)^5 + p_4 \cos(\beta)^4 + p_3 \cos(\beta)^3 + p_2 \cos(\beta)^2 + p_1 \cos(\beta) + p_0$	0.0078

(H_s) and $M_p\ (V)$, while a two-term sinusoid, a summation of cosines and linear term, and a 4th and 6th order polynomials (similar to the 4th and 6th order Taylor series expansion for cosine) were used for $M_p\ (\beta)$. The goodness of fit is evaluated in terms of the root mean square error (RMSE) for each of the function for $M_p\ (H_s)$, $M_p\ (V)$, and $M_p\ (\beta)$ and listed in Table 3.1. In Fig. 3.2 the functions B_2, B_3, and B_4 lie on top of each other and fit the data points with a RMSE of less than 1.0E−4.

Based on the performance of the proposed functions for $M_P(H_s)$, $M_p(V)$, $M_P(\beta)$ as presented in Table 3.1, two nonlinear prediction surfaces are proposed. The first includes 2nd order polynomial functions for $M_P(H_s)$ and $M_p(V)$ (i.e. A_2 and B_2) and the summation of cosines and linear term for $M_P(\beta)$ (i.e. C_2). These functions were chosen in order to minimize the number of coefficients, p_i, while also having a low RMSE. The first nonlinear prediction surface takes the form

$$\Psi^{nonlin} = p_1 {H_s}^2 + p_2 H_s + p_3 + p_4 V^2 + p_5 V + p_6 \cos(\cos(\beta)) - p_7 \cos(p_8 \cos(\beta)) + p_9 \cos(\beta) \tag{3.14}$$

The second proposed nonlinear prediction surface restricts itself to the use of polynomial functions for H_s, V, and $\cos(\beta)$. The 2nd order polynomial functions A_2 and B_2 are used as the contributions for $M_P(H_s)$ and $M_p(V)$, respectively, and the 4th order polynomial (i.e. C_3) is used to account for $M_P(\beta)$. The polynomial based nonlinear prediction surface takes the form

$$\Psi^{nonlin-poly} = p_1 {H_s}^2 + p_2 H_s + p_3 + p_4 V^2 + p_5 V + p_6 \cos(\beta)^4 + p_7 \cos(\beta)^3 + p_8 \cos(\beta)^2 + p_9 \cos(\beta) \tag{3.15}$$

3.4 Application and Results

The HSV-2 Swift is an aluminum naval vessel which was instrumented with strain gauges and various other sensors for seakeeping trials. The ship was operated by systematically varying ship speeds and heading angles in different sea states [16]. The T2-4 sensor is located at a fatigue critical location on the HSV-2 Swift to specifically capture stresses induced by vertical bending. The SHM data for the T2-4 sensor were processed and fit with Eqs. (3.1) and (3.2). As a result, for each cell, the parameter set $\{A_{LF}, B_{LF}, A_{HF}, B_{HF}\}$ fully defines the structural response if Eq. (3.1) is used, and, $\{C_{LF}, D_{LF}, E_{LF}, C_{HF}, D_{HF}$, and $E_{HF}\}$ if Eq. (3.2) is used. In order to predict the response in missing cells, all parameters within the set must be extrapolated.

The performance of the nonlinear surfaces is first investigated with respect to their ability to capture the variation in the observed data. That is, all parameters in sets $\{A_{LF}, B_{LF}, A_{HF}, B_{HF}\}$ and $\{C_{LF}, D_{LF}, E_{LF}, C_{HF}, D_{HF}$, and $E_{HF}\}$, for Ψ^{lin}, Ψ^{nonlin}, and $\Psi^{nonlin\text{-}poly}$ are fit to the available data points and the mean square error (MSE) is calculated. This process is shown in Fig. 3.3 for C_{LF}. The data points for C_{LF} are plotted as a function of wave height and heading angle for a constant ship speed in Fig. 3.3a and as a function of ship speed and wave height for a constant heading angle in Fig. 3.3b. Figure 3.3a and b also show the fitted surfaces for Ψ^{lin}, Ψ^{nonlin}, and $\Psi^{nonlin\text{-}poly}$. The surfaces for Ψ^{nonlin} and $\Psi^{nonlin\text{-}poly}$ lie on top of each other in Fig. 3.3a and b and have comparable MSE, as listed in Table 3.2. The results for the MSE for Ψ^{lin}, Ψ^{nonlin}, and $\Psi^{nonlin\text{-}poly}$ for all parameters are listed in Table 3.2; similar figures can be generated for all other parameters but are omitted for brevity.

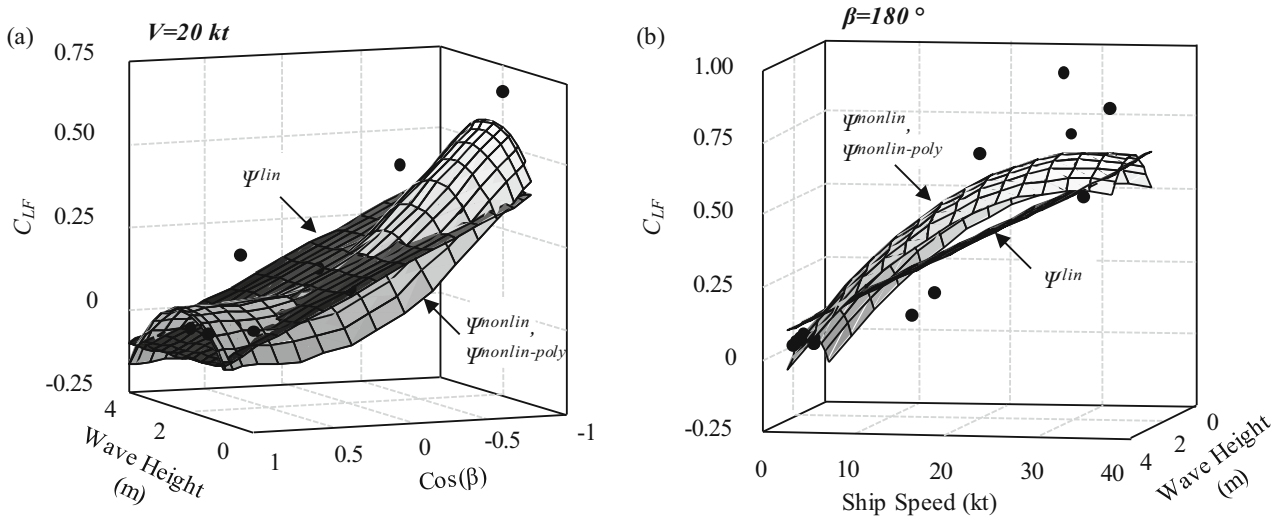

Fig. 3.3 Available data points for the response parameter C_{LF} (shown as *black* points) and the fitted surfaces for Ψ^{lin}, Ψ^{nonlin}, and $\Psi^{nonlin\text{-}poly}$ where (**a**) shows the variation of C_{LF} with wave height and heading angle for a ship speed of 20 kts and (**b**) shows the variation of C_{LF} with ship speed and wave height for a heading angle of 180°

Table 3.2 Evaluation of proposed surfaces with respect to observed data

Parameter	Mean square error Ψ^{lin}	Mean square error Ψ^{nonlin}	Mean square error $\Psi^{nonlin\text{-}poly}$	Parameter	Mean square error Ψ^{lin}	Mean square error Ψ^{nonlin}	Mean square error $\Psi^{nonlin\text{-}poyl}$
A_{LF}	0.022	0.022	0.020	C_{LF}	0.034	0.028	0.028
B_{LF}	0.034	0.022	0.017	D_{LF}	0.022	0.012	0.012
A_{HF}	0.103	0.099	0.099	E_{LF}	0.008	0.008	0.008
B_{HF}	0.083	0.087	0.086	C_{HF}	0.175	0.163	0.161
				D_{HF}	0.048	0.046	0.046
				E_{HF}	0.005	0.005	0.004

The theoretically-based nonlinear prediction surfaces typically outperform the linear surface for all low frequency parameters. The high frequency parameters show minimal or no improvement when compared to the linear surface. This can be attributed to the fact that the surfaces were developed based on wave bending moment, which is governed by the low frequencies. Slam impacts typically govern the high frequency response and would thus be better predicted by alternative nonlinear relationships.

The performance of the nonlinear surfaces is also investigated with respect to their ability to predict unobserved responses. In order to evaluate the performance of the prediction surfaces, data was removed from the initial data set (which includes all available sea trials). The data that was removed is referred to as the missing data set, while the remaining data is referred to as the available data set. Cases considering 70% available data and 50% available data were tested for predicting parameters in the sets $\{A_{LF}, B_{LF}, A_{HF}, B_{HF}\}$ and $\{C_{LF}, D_{LF}, E_{LF}, C_{HF}, D_{HF}$, and $E_{HF}\}$. C_{LF} is presented for further discussion; others are available but are omitted for brevity. Results of the prediction are shown in Table 3.2.

Ten sets of available data are included as representative data sets. Available data set 1 refers to the case of no missing data and it was found that Ψ^{nonlin} and $\Psi^{nonlin\text{-}poly}$ outperform Ψ^{lin}. The 70% available data and 50% available data cases are chosen randomly so as not to impart bias onto the available data set. Available data sets 2–5 use 70% of the available data and sets 6–10 use 50% available data. It can be seen that Ψ^{nonlin} and $\Psi^{nonlin\text{-}poly}$ outperforms Ψ^{lin} for available data sets 2–5 (i.e. 30% missing data) as shown in Table 3.3. The same can be said for available data sets 6–10 (i.e. 50% missing data).

Ψ^{nonlin} and $\Psi^{nonlin\text{-}poly}$ typically perform comparably for all available data sets. However, in some 50% available data cases, local fluctuations in the prediction surface can occur with Ψ^{nonlin} as shown in Fig. 3.4. While the MSE for Ψ^{nonlin} and $\Psi^{nonlin\text{-}poly}$ for available data set 6 are similar, $\Psi^{nonlin\text{-}poly}$ fits the overall trend while avoiding the local fluctuations shown in Fig. 3.4a. While such fluctuations in the surface Ψ^{nonlin} do not have a substantial impact on this specific case, they may have large impact on other case studies.

Table 3.3 MSE for predicting Parameter C_{LF} as a function of missing data

Available data set	Percent available data	Mean square error Ψ^{lin}	Mean square error Ψ^{nonlin}	Mean square error $\Psi^{nonlin\text{-}poly}$
1	100	0.034	0.028	0.028
2	70	0.034	0.029	0.029
3	70	0.035	0.031	0.031
4	70	0.034	0.030	0.031
5	70	0.035	0.029	0.029
6	50	0.035	0.030	0.034
7	50	0.036	0.032	0.032
8	50	0.034	0.029	0.029
9	50	0.034	0.030	0.031
10	50	0.039	0.033	0.039

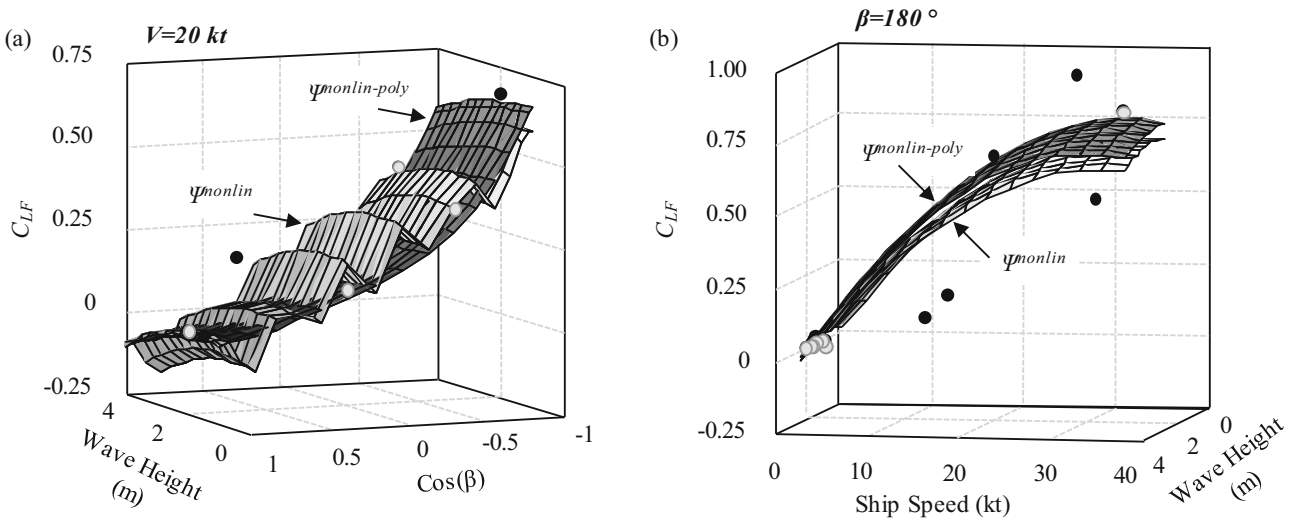

Fig. 3.4 Available data points for the response parameter C_{LF} (shown as *black* points), missing data points (shown in *light grey*), and the fitted surfaces for Ψ^{lin}, Ψ^{nonlin}, and $\Psi^{nonlin\text{-}poly}$ for available data set 6; (**a**) shows the variation of C_{LF} with wave height and heading angle for a ship speed of 20 kts and (**b**) shows the variation of C_{LF} with ship speed and wave height for a heading angle of 180°

3.5 Conclusions

Theoretically-based nonlinear prediction surfaces for the response of naval vessels under varying operational conditions are proposed and evaluated with respect to the structural response of the HSV-2 Swift. The nonlinear prediction surfaces are based on the theoretical relationships between the operational condition given in terms of the wave height, ship speed, and heading angle, and the ship response in terms of the vertical bending moment as derived from linear strip theory. Two theoretically-based nonlinear prediction surfaces are proposed and compared with linear prediction surfaces; both outperform linear surfaces in estimating low frequency response characteristics. For high frequency characteristics, the nonlinear and linear surfaces are comparable in their performance with linear surfaces occasionally outperforming the nonlinear ones. This is due to the fact that the nonlinear surfaces were developed based on the theoretical relationships of wave bending moments, which are governed by the low frequencies. However, slam impacts typically govern the high frequency response. The development of a separate surface for high frequency parameters which would focus on impact and slam loads may provide further enhancement to the prediction of the overall response. Additionally, the accuracy of the recorded SHM data is not included in the proposed methodology, which may contribute to the error in the developed surfaces.

Acknowledgments The support by grants from (a) the National Science Foundation (NSF) Award CMMI-1537926, (b) the U.S. Office of Naval Research (ONR) Awards N00014-08-1-0188, N00014-12-1-0023, and N00014-16-1-2299, and (c) the National Aeronautics and Space Administration (NASA) Award NNX10AJ20G is gratefully acknowledged. The opinions presented in this paper are those of the authors and do not necessarily reflect the views of the sponsoring organizations.

References

1. Lynch, J.P., Loh, K.J.A.: Summary review of wireless sensors and sensor networks for structural health monitoring. Shock Vib. Digest. **38**(2), 91–130 (2006)
2. Zhu, J., Collette, M.A.: Bayesian approach for shipboard lifetime wave load spectrum updating. Struct. Infrastruct. Eng. **13**(2), 298–312 (2016)
3. Kurata, M., Kim, J.H., Lynch, J.P., Law, K.H. and Salvino, L.W.: A probabilistic model updating algorithm for fatigue damage detection in aluminum hull structures. In: ASME 2010 Conference on Smart Materials, Adaptive Structures and Intelligent Systems, pp. 741–750. American Society of Mechanical Engineers, New York (2010)
4. Zhu, B., Frangopol, D.M.: Reliability assessment of ship structures using Bayesian updating. Eng. Struct. **56**, 1836–1847 (2013)
5. Frangopol, D.M., Strauss, A., Kim, S.: Bridge reliability assessment based on monitoring. J. Bridg. Eng. **13**(3), 258–270 (2008)
6. Hughes, O.F.: Ship Structural Design: A Rationally-Based, Computer-Aided, Optimization Approach. Wiley-Interscience, Jersy City (1983)
7. Sikora, J.P., Dinsenbacher, A., Beach, J.E.: A Method for estimating lifetime loads and fatigue lives for swath and conventional monohull ships. Nav. Eng. J. **95**(3), 63–85 (1983)
8. Kim, S., Frangopol, D.M.: Cost-effective lifetime structural health monitoring based on availability. J. Struct. Eng. **137**(1), 22–33 (2010)
9. Iphar, C., Napoli, A. and Cyril, R.: Data quality assessment for maritime situation awareness. In: ISSDQ 2015-The 9th International Symposium on Spatial Data Quality, vol. 2, pp. 291–296. (2015).
10. Zhu, J.: Life cycle fatigue management for high-speed vessel using Bayesian updating approaches. Ph.D. thesis, Dept. of Naval Architecture and Marine Engineering, University of Michigan, Michigan, USA (2014)
11. Mondoro, A., Soliman, M., Frangopol, D.M.: Prediction of structural response of naval vessels based on available structural health monitoring data. Ocean Eng. **125**, 295–307 (2016)
12. Pierson Jr., W.J., Moskowitz, L.: A proposed spectral form for fully developed wind seas based on the similarity theory of SA Kitaigorodskii. J. Geophys. Res. **69**(24), 5181–5190 (1963)
13. Komen, G.J., Hasselmann, K., Hasselmann, K.: On the existence of a fully developed wind-sea spectrum. J. Phys. Oceanogr. **14**(8), 1271–1285 (1984)
14. Jensen, J.J., Mansour, A.E.: Estimation of ship long-term wave-induced bending moment using closed-form expressions. R. Inst. Nav. Archit. Trans. Part A. Int. J. Marit. Eng. 41–55 (2002)
15. Jensen, J.J., Mansour, A.E., Olsen, A.S.: Estimation of ship motions using closed-form expressions. Ocean Eng. **31**(1), 61–85 (2004)
16. Brady, T., Bachman, R., Donnelly, M., Griggs, D.: HSV-2 Swift Instrumentation and Technical Trials Plan. Naval Surface Warfare Center, Carderock Division (NSWCCD), West Bethesda (2004)